Luminescent Nd3+, Cr3+ codoped YAG nanocrystals for thermal sensing: Influence of the excitation wavelength

Geraldine Dantelle, Valérie Reita, Alain Ibanez, Gilles Ledoux, Christophe Dujardin

Version of Record: https://www.sciencedirect.com/science/article/pii/S0921452621007705
Manuscript_833a33bb3e9ba05290feb86b8ccdc1f9

Luminescent Nd^{3+}, Cr^{3+} codoped YAG nanocrystals for thermal sensing: influence of the excitation wavelength.

Géraldine Dantelle[1*], Valérie Reita[1], Alain Ibanez[1], Gilles Ledoux[2], Christophe Dujardin[2]

[1] Univ. Grenoble Alpes, CNRS, Grenoble INP, Institut Néel, 38000 Grenoble, France
[2] Univ. Lyon, Univ. Claude Bernard Lyon 1, CNRS, Institut Lumière Matière, F-69622, VILLEURBANNE, France

[*]Corresponding author: geraldine.dantelle@neel.cnrs.fr

Abstract:
$Y_3Al_5O_{12}$ (YAG) nanocrystals codoped with Nd^{3+} and Cr^{3+} ions have been produced by a modified solvothermal method. The incorporation of both Nd^{3+} and Cr^{3+} inside the YAG network has been attested by X-ray diffraction and photoluminescence measurements. Modification of the excitation wavelength leads to ratiometric intensity changes between the luminescence attributed to Nd^{3+} and that of Cr^{3+}. Temperature-dependent luminescence spectra have been analyzed according to the different excitation wavelengths. The highest relative thermal intensity ($S_r = 2.5$ %.K^{-1}) is obtained under a 532 nm excitation, which favors the direct and independent excitation of Cr^{3+} and Nd^{3+}.

Keywords: luminescence, nanothermometry, YAG nanocrystals, lanthanide, transition metal ion, thermal sensing

1. Introduction

Luminescence nanothermometry consists in measuring the temperature at the nanoscale without using contact probes which can, at this scale, affect the measurement. Although it was used in the early 2000s for hot spot localization in micro-electronic circuits [1,2], it has recently experienced a renewed interest because of its forecast applications in bio-medicine and biology [3,4]. Indeed, the possibility to access to local temperature at the cellular level paves the way to numerous applications, such as the detection of inflammatory areas (a few degrees hotter than non-inflammatory zones) or the monitoring of hyperthermia. In this latter case, the challenge is to kill cancerous cells by a local temperature increase of a few degrees, while avoiding damaging healthy cells. If the temperature increase is achieved by using metallic or magnetic nanoparticles, which can dissipate heat upon light illumination or magnetic field irradiation respectively, there is a strong need to develop nanothermometers that will be used as probes to finely monitor the local temperature at the cellular level and avoid any collateral damage [5]. In addition, intracellular nanothermometry appears highly challenging to get a better understanding of cellular physiology and metabolism, including the mitochondrial activity and its controversial temperature variation related to energy production [6,7].

The development of luminescent nanothermometers, that can address these challenges, has strongly boomed over the last years. Such nanothermometers have to fulfill numerous specifications, including (1) a high temperature sensitivity, essential to obtain a robust temperature measurement with a minimum uncertainty, (2) a strong photoluminescence efficiency, also contributing to minimize the temperature uncertainty, (3) a good biocompatibility and an efficient cell uptake (and even mitochondrial uptake for intracellular study) and blood circulation and (4) a low sensitivity to others parameters (pH, ionic concentration, etc).

Luminescence nanothermometry can be based on various temperature-dependent processes [8,9]: variation of excited state lifetime or of luminescence intensity, spectral shift of luminescence, etc. Among these different mechanisms, ratiometric measurements, based on the relative intensity variation of two luminescence peaks, are particularly robust and reliable as they provide relatively high thermal sensitivities and can be implemented on classical fluorescence imaging set-up. For this ratiometric luminescence nanothermometry, different types of nanomaterials have been proposed, from organic compounds (such as thermoresponsive molecular micro/nano-gels [10], molecular nanothermometers [11,12], fluorescent proteins [13]) to organic-inorganic hybrids (polyoxometallates [14], metal-organic frameworks [15]) and purely inorganic particles (lanthanide-doped $NaYF_4$ [16,17], CdTe quantum dots [18], Bi^{3+}/Cr^{3+}-doped $ZnGa_2O_4$ particles [19] etc).

In the context of bio-medicine, lanthanide-doped nanocrystals appear particularly interesting as they provide numerous narrow luminescence peaks, including some in the near-infrared range, allowing fluorescence filtering in the biological transparency regions, which should be considered for *in vivo* thermometry measurements. In particular, Nd^{3+}-doped nanocrystals ($CaF_2:Nd^{3+}$ [20], $LaF_3:Nd^{3+}$ [21], $Y_3Al_5O_{12}:Nd^{3+}$ [22], $Gd_3Sc_2Al_3O_{12}:Nd^{3+}$ [23], etc) have

attracted attention. The temperature sensing is based on the variation of luminescence intensity (I_1 and I_2) of two thermally-coupled emission peaks of Nd^{3+}, corresponding to the Stark sublevels of $F_{3/2} \rightarrow I_{9/2}$ electronic transition of Nd^{3+}. A luminescence intensity ratio (LIR), defined as $LIR = \frac{I_1}{I_2}$, is thus measured as a function of temperature and leads to the assessment of a relative thermal sensitivity calculated as $S_r = \frac{1}{LIR}\frac{dLIR}{dT}$.

LIR is directly related to the excited state population of the considered emitting sublevels of Nd^{3+}, as defined from Boltzmann equilibrium [24]. S_r is thus directly related to the energy difference of the emitting Stark sublevels, which is not significantly affected by crystal field for intra-configurational f-f transitions. As a result, in most of the studied matrices, the relative thermal sensitivity is quite similar, around 0.1 - 0.2 $\%.K^{-1}$, with a temperature uncertainty around 0.5 K. [20,21,22,23] Nonetheless, a higher S_r value (0.58 $\%.K^{-1}$) was recently found in Nd^{3+}-doped $LiLuF_4$ nanocrystals when taking into account very accurate spectral ranges that contain additional spectral shift and line broadening [25].

In order to enhance the relative thermal sensitivity, new approaches have been developed, that do not only rely on Boltzmann's population equilibrium [26]. The first approach is based on monitoring the luminescence intensity of peaks arising from distinct lanthanide doping ions, promoted to their excited states through temperature-dependent energy transfers. For instance, in the case of a Nd^{3+},Yb^{3+} co-doping, Yb^{3+} ions are first excited upon a NIR excitation and then promoting Nd^{3+} ions to their excited levels by phonon-assisted energy transfers [27]. As the energy transfer depends directly on temperature (phonons), thermal sensing is achieved by monitoring Yb^{3+} and Nd^{3+} luminescence peaks, with S_r of 0.4 $\%.K^{-1}$ [28]. Such strategy requires a fine optimization of both Nd^{3+} and Yb^{3+} concentration and the appropriate choice of the host matrix, which should present phonons with suitable energy to promote energy transfer. It also involves a genuine material engineering at the nanoscale, with the successive synthesis of shells containing appropriate doping ions to avoid any unwanted cross-relaxation processes between lanthanide ions. An example is given by Skripka *et al.* who prepared core/shell/shell fluoride nanocrystals composed of successive layers containing different lanthanide ions [29]. The core doped with Ho^{3+} and Er^{3+} presents a luminescence, peaking around 1.2 µm and 1.5 µm respectively, whose intensity increases with temperature thanks to phonon-assisted energy transfer, whereas the luminescence of the outer layer doped with Nd^{3+} decreases. The maximal S_r, obtained from thermal variation of LIR calculated from the Er^{3+}/Nd^{3+} or Ho^{3+}/Nd^{3+} pairs, reaches 1.1 $\%.K^{-1}$.

The second strategy, widely developed by Marciniak *et al.* in recent papers based on nanostructured oxide particles consists in codoping crystals ($LiLaP_4O_{12}$, $LiAl_5O_8$, garnets) with one lanthanide ion (Nd^{3+}, Eu^{3+}) and one transition metal ion (Cr^{3+}, Fe^{3+}, Ti^{4+}, Mn^{4+}) to benefit from the different thermal behavior of each of these doping ions of different nature [30,31,32,33,34]. Maximal relative thermal sensitivities of a few $\%.K^{-1}$ are reported in those publications, about one order of magnitude higher than in the Nd^{3+} single-doped crystals. However, several parameters influence the thermal sensitivity of the codoped

nanothermometers: the nature of the host matrix, the lanthanide concentration, the transition metal ion concentration, the temperature, the excitation wavelength, the possibility of energy transfer between both doping ions, the crystallite size, etc. This makes difficult to understand physical processes underlying these high thermal sensitivities and hard to predict the best nanothermometer performances. As a consequence, a thorough optimization of each system is needed [35,36,37].

In the context of the second strategy, this paper reports on the nanothermometry properties of YAG nanocrystals codoped with Nd^{3+} and Cr^{3+} under different excitation wavelengths. Garnet compounds are particularly appropriate for such a study as they can accommodate both lanthanide ions, which can easily substitute Y^{3+} ions, and transition metal ions, which can substitute Al^{3+} ions. Such YAG nanocrystals were synthesized through a modified solvothermal method [38], to ensure high crystal quality along with a very low aggregation state.

2. Material and methods

2.1. Materials synthesis

Nd^{3+},Cr^{3+}-codoped YAG nanocrystals were synthesized according to the following procedure: 2.45 mmol $Y(CH_3COO)_3 \bullet 4H_2O$ (Alfa Aesar, 99.9 %), 0.05 mmol $Nd(CH_3COO)_3 \bullet 4H_2O$ (Sigma Aldrich, 99.9 %), 0.021 mmol $Cr(CH_3COO)_3$, hydrate (Strem, 97 %) and 4.15 mmol $Al(CH(CH_3)_2)_3$ (Alfa Aesar, 98%), with a minimal purity of 99.9 %, were mixed in 1,4-butanediol (18 mL, Sigma, 99 %). The stoichiometry, corresponding to the nominal phase $Y_{2.94}Nd_{0.06}Al_{4.975}Cr_{0.025}O_{12}$ (also labelled YAG:2%Nd,0.5%Cr), was chosen based on previously published results [36,39]. In addition, single doped YAG nanocrystals (YAG:2%Nd and YAG:0.5%Cr) were synthesized in the same way.

After stirring the mixture for 5 days, a gel-like solution was obtained. 1 mL was introduced in a sapphire tube, blocked with two pistons and pressurized with He gas. The tube was introduced in a home-designed autoclave [40], allowing to operate under constant pressure (200 bar) and temperature (400°C). The reaction time was set for 2.5 hours. After cooling down, the solution was retrieved, washed three times in ethanol by successive centrifugations and dried at room temperature for 24 hours.

2.2. Structural characterizations

Powder X-ray diffraction (PXRD) pattern was recorded on a Siemens D8 Advance diffractometer (λ_{Cu} = 1.54056 Å), in the 2θ 15-75° range. The unit cell parameter and the coherence length were determined using the Le Bail method. Nanocrystal size and morphology were investigated by Transmission Electron Microscopy (TEM, Philips CM300, 300 kV).

2.3. Optical characterizations

Photoluminescence spectra were recorded at room temperature and in the temperature range 25-45 °C, using a micro-setup (objective: x50, NA: 0.55) coupled with a temperature stage (Linkam THMS600). The excitation was performed using a CW Argon laser (488 nm and 514 nm, typical power: 1 mW) or a 532-nm diode laser (Cobolt, typical power: 1 mW) and focused

on the sample through an Olympus objective (x 50, NA: 0.55). The emission was collected through the same microscope objective and detected, after a razor edge filter at 532 nm, through a T6400 spectrometer (Horiba) equipped with a Symphony Camera detector cooled at 77 K. Luminescence measurements were performed using a diode pumped 50 Hz tunable OPO laser from EKSPLA (NT230-50-SH) as excitation source. The laser can be continuously tuned between 215 and 2500 nm and has laser pulses shorter than 3 ns. A beam sampler is interposed and the sampled beam is fed to a pyroelectric energy sensor 919E-10-24-10K from Newport to monitor the pulse-by-pulse energy variation. The rest of the laser beam is used to excite the sample. The emission is then collected by an optical fiber and fed to a monochromator coupled with an EMCCD (respectively Kymera 328i and Newton both from ANDOR technologies). The excitation spectra are obtained by varying the laser wavelength and integrating the EMCCD collected light over a range of wavelengths. For luminescence lifetime measurements a second fiber also collects the luminescence and is fed to a monochromator (TRIAX320 from Hamamatsu) coupled with a R2949 Peltier cooled photomultiplier tube from Hamamatsu. Photon arrival times are histogrammed by an MCS6A multichannel scaler from Fast ComTec with a temporal with the time per bin set to 6.55 µs.

3. Results

3.1. Nd^{3+},Cr^{3+}-codoped YAG structure and morphology

Pure Nd^{3+},Cr^{3+}-codoped YAG nanocrystals are obtained, as attested by PXRD (**Figure 1a**). The Le Bail fit gives a unit cell parameter *a* of 12.081 Å, which is higher than the unit cell parameter of single doped Nd^{3+} YAG nanocrystals (2 mol.% Nd^{3+}) elaborated by the same method (*a* = 12.035 Å [23]). The difference attests from the effective incorporation of Cr^{3+}, which presents a larger ionic radius than Al^{3+} (r_{Cr3+} = 0.615 Å vs. r_{Al3+} = 0.535 Å in a six-fold coordinated environment). The coherence length, also determined from the Le Bail fit, is 190 ± 20 nm.
TEM observations show nanocrystals with an average size of 170 nm (**Figure 1b**), which is similar to the measured coherence length and suggests that each nanoparticle consists of a single-crystal. In addition, some particles present faceted edges (**Figure 1c**) and, at high magnification, atomic planes running up to the particle edges can be observed, confirming the good crystal quality of the particles.

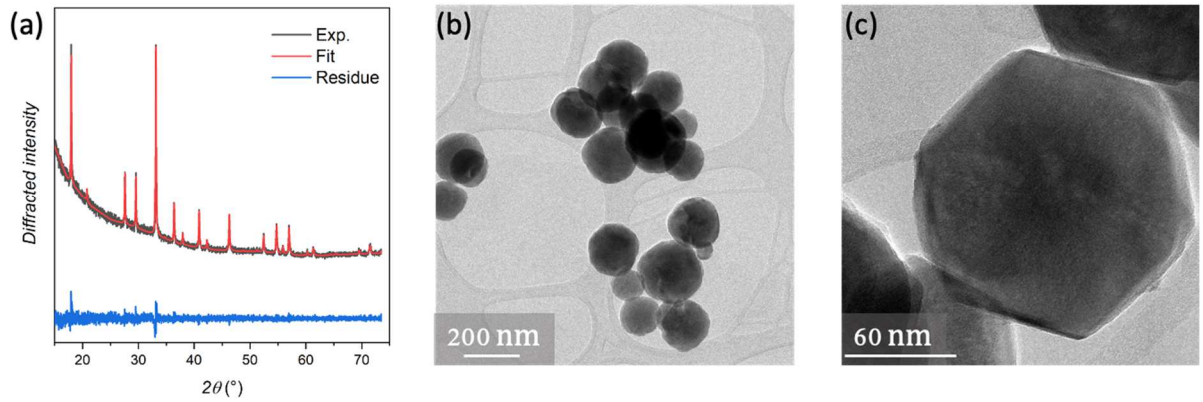

***Figure 1**: (a) Powder X-ray diffraction pattern of Nd^{3+},Cr^{3+}-codoped YAG nanocrystals. (b-c) TEM images of Nd^{3+},Cr^{3+}-doped YAG nanocrystals recorded at different magnifications.*

3.2. Luminescence spectra

Luminescence spectra of Nd^{3+},Cr^{3+}-codoped YAG particles were recorded under different excitation wavelengths (488 nm, 514 nm and 532 nm) and are shown on **Figure 2a**. Under all excitation wavelengths, both Cr^{3+} and Nd^{3+} luminescence peaks are observed. The Cr^{3+} luminescence signature consists in the sharp luminescence peak at 689 nm corresponding to the spin-forbidden $^2E \rightarrow {}^4A_2$ transition, another narrow peak at 702 nm corresponding the vibronic sideband and a broad luminescence centered at 705 nm corresponds to the spin-allowed $^4T_2 \rightarrow {}^4A_2$ transition, with associated Stokes and anti-Stokes broadening (**Figure 2c**) [41]. The Nd^{3+} luminescence corresponds to $^4F_{3/2} \rightarrow {}^4I_{9/2}$ transition (from 865 to 950 nm), and more specifically to R_1, R_2 Stark sublevels of $^4F_{3/2}$ to the different Z_1, …, Z_5 Stark sublevels of $^4I_{9/2}$ (**Figure 2c**). According to the excitation wavelength, the luminescence intensity ratio between the Nd^{3+} and Cr^{3+} luminescence signature varies, as shown in **Figure 2b** for which the intensity of the narrow Cr^{3+} peak at 689 nm and the intensity of the 945 nm peak for Nd^{3+} are considered. It indicates that the efficiency of the excitation mechanisms of both Cr^{3+} and Nd^{3+} changes with the excitation wavelength, as discussed below.

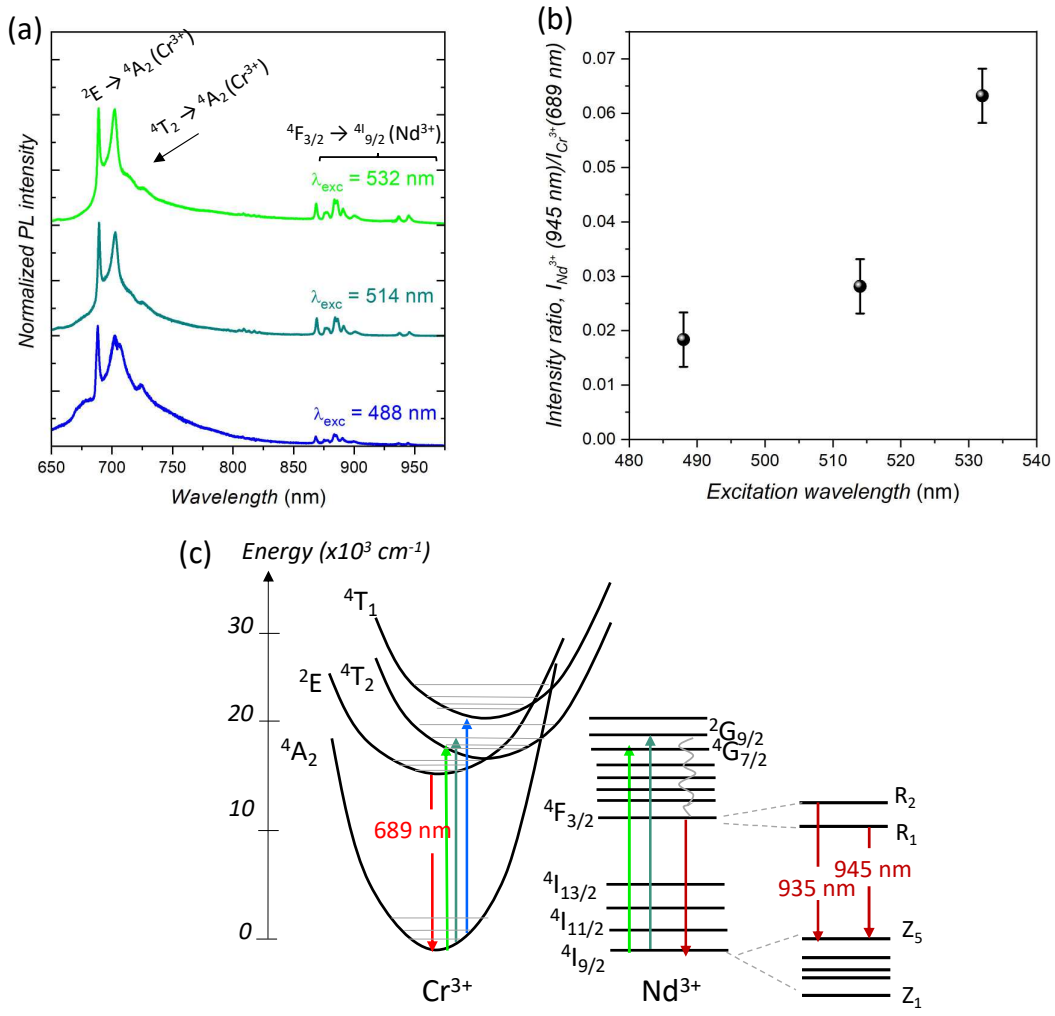

***Figure 2**: (a) Room temperature luminescence spectra of Nd^{3+},Cr^{3+}-codoped YAG nanocrystals as a function of the excitation wavelengths, λ_{exc} = 488 nm (blue), 514 nm (dark green), 532 nm*

(green). (b) Variation of the intensity ratio between the luminescence peak of Nd^{3+} at 945 nm and that of Cr^{3+} at 689 nm, according to the excitation wavelength. (c) Simplified energy level diagram of Cr^{3+} and Nd^{3+} in the YAG host matrix.

3.3. Temperature-dependence luminescence spectra

Luminescence spectra were recorded with the temperature variation in the physiological range (25 - 45°C) under the different excitation wavelengths (as shown in **Figure 3a** for a 532-nm excitation). Considering only the Nd^{3+} luminescence peaks, and particular the two peaks corresponding to the (R_1, R_2) $\rightarrow$ Z_5 transitions at 935 and 945 nm (**Figure 2c**) for the measurement of the LIR corresponding, a S_r value of 0.10 %.K^{-1} is obtained, as already measured in single-doped Nd^{3+} YAG nanocrystals [23]. This is consistent with the fact that the thermal sensing is governed by the energy gap (typically around 100 cm^{-1}) between the R_1 and R_2 sublevels, whose population follows the Boltzmann equilibrium. When considering only the emission of Cr^{3+}, e.g. at 725 nm and 845 nm, the linear LIR evolution with temperature leads to a S_r value of 0.06 %.K^{-1}.

As both Nd^{3+} and Cr^{3+} ions present a different thermal behavior due to their intrinsic nature, a new LIR is defined considering the luminescence peak of Nd^{3+} at 945 nm and of Cr^{3+} at 689 nm:

$$LIR = \frac{I_{Nd3+(945\ nm)}}{I_{Cr3+(689\ nm)}}$$

It is worth noting that other luminescence peaks could have been considered. The choice of these peaks was driven by the fact that they are spectrally well-separated, which allows a good discrimination, and they are narrow which could ease their filtering. In addition, these emission peaks lie within the first biological transparency window, defined between 650 and 950 nm, [42], which is of great advantage for *in vivo* measurements.

The LIR evolution with temperature is presented in **Figure 3b** for the different excitation wavelengths. From the slope $\frac{dLIR}{dT}$ and the LIR value at 25°C, the S_r values are calculated: S_r = 0.8 %.K^{-1} for a 488-nm excitation, S_r =1.8 %.K^{-1} for a 514-nm excitation and S_r = 2.5 %.K^{-1} for a 532-nm excitation.

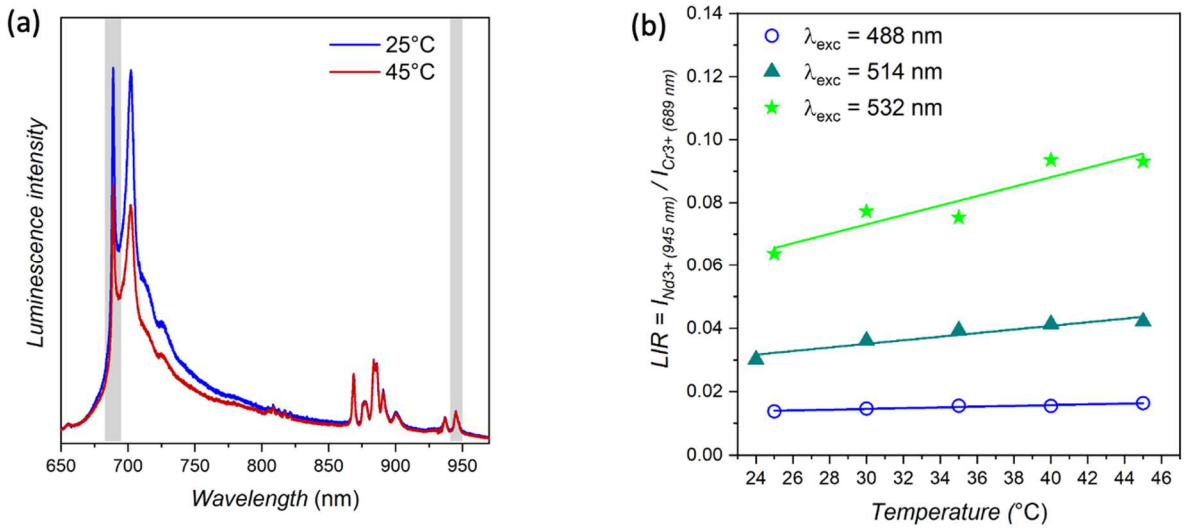

***Figure 3**: (a) Luminescence spectra of Nd^{3+},Cr^{3+}-codoped YAG nanocrystals at 25°C (blue) and 45°C (red) under a 532-nm excitation. For sake of comparison, both spectra were normalized on the 945-nm peak. (b) Evolution of LIR as a function of temperature for different excitation wavelengths, λ_{exc} = 488 nm (blue dots), 514 nm (dark green triangles), 532 nm (green stars).*

4. Discussion

These results show that the relative thermal sensitivity S_r of Nd^{3+},Cr^{3+}-codoped YAG nanocrystals is much higher than the one obtained for single-doped Nd^{3+} nanocrystals, by one order of magnitude. In addition, they also reveal the important effect of the excitation wavelength on the S_r value of codoped samples: the best S_r value (2.5 %.K^{-1}) is obtained under the 532 nm excitation, whereas S_r is 3 times lower for the 488 nm excitation. In a recent paper, Marciniak *et al.* suggested that the origin of the difference of thermal sensitivity in Nd^{3+},Cr^{3+}-codoped samples originates from excitation mechanisms of both Nd^{3+} and Cr^{3+} varying with the excitation wavelength [36]. They proposed to distinguish the 2 following situations: (1) when the excitation allows for the direct and independent excitation of Cr^{3+} and Nd^{3+}, the thermal sensitivity is governed by the temperature dependent luminescence intensity of Nd^{3+} and of Cr^{3+} separately; (2) When the excitation of one of the codoping ions occurs through energy transfer, the thermal sensitivity depends on the variation of the energy transfer efficiency with temperature.

To confirm this hypothesis, we investigate and discuss here the possibility of direct excitation of Nd^{3+} and Cr^{3+} as a function of the excitation wavelength, along with the potential energy transfer between Cr^{3+} and Nd^{3+}. Excitation spectra of both Nd^{3+},Cr^{3+}-codoped YAG and Nd^{3+}-doped YAG nanocrystals was recorded by monitoring Nd^{3+} emission at 892 nm (**Figure 4a**). Although all considered excitation wavelengths (488, 514 and 532 nm) allow for direct excitation of Nd^{3+} ions, it is clear that the 532-nm excitation, populating the $^4G_{7/2}$,$^2G_{9/2}$ levels of Nd^{3+} [43,44], is much more appropriate for efficient excitation of Nd^{3+} than that at 488 nm. These excitation spectra are in good agreement with the absorption spectrum of Nd^{3+}-doped YAG single-crystals [45]. Regarding Cr^{3+} ions, all considered excitation wavelengths allow for their direct excitation (**Figure 4a**) [41].

To assess the possibility of energy transfer from Cr^{3+} to Nd^{3+} ions, the luminescence decay curves of both Nd^{3+},Cr^{3+}-codoped and Cr^{3+}-doped YAG nanocrystals were recorded under 488- and 532-nm excitation (**Figure 4b**). Under both excitation wavelengths, Cr^{3+} luminescence lifetime is shortened by a factor of 2 when Nd^{3+} ions are present, which attests from non-radiative energy transfers from Cr^{3+} to Nd^{3+}.

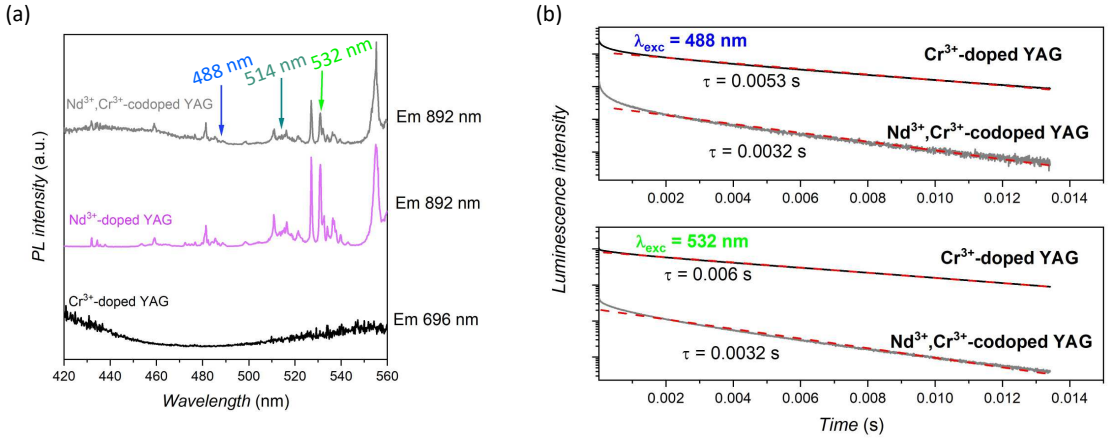

***Figure 4**: (a) Excitation spectra of Nd^{3+}-doped YAG nanocrystals (purple) and Nd^{3+},Cr^{3+}-doped YAG nanocrystals (grey) when observing the Nd^{3+} emission at 892 nm and of Cr^{3+}-doped YAG nanocrystals (black) when observing the Cr^{3+} emission at 696 nm. (b) Luminescence decay curves recorded at 696 nm for Cr^{3+}-doped YAG nanocrystals (black) and Nd^{3+},Cr^{3+}-doped YAG nanocrystals (grey), with associated fits (red dashed lines) under a 488- and 532-nm excitation.*

Hence, for both 488- and 532-nm excitations, two Nd^{3+} excitation pathways exist: energy transfer from Cr^{3+} and direct excitation. However, this latter is less probable under the 488-nm excitation than under the 532-nm excitation (**Figure 4a**). At 488 nm, the main excitation pathway for Nd^{3+} ions is probably the energy transfer mechanism, which thus governs the thermal sensitivity. On the other hand, at 532 nm, the direct excitation plays a more significant role, leading to a thermal sensing process based on the difference of thermal quenching of Cr^{3+} and of Nd^{3+} in the considered temperature range. This evolution confirms the interpretation proposed by Marciniak *et al.* [36]. Exciting directly Cr^{3+} and Nd^{3+} ions leads to a higher temperature sensitivity as the thermal dependence of Cr^{3+} luminescence in this temperature range is stronger than the one of Nd^{3+}, whose luminescence signal remains nearly constant. It should be noted that the temperature dependence of the energy transfer rate between Cr^{3+} and Nd^{3+} has been measured nearly constant in YAG ceramics [46,47], indicating that the temperature readout process cannot be based on energy transfer only.

Hence, Nd^{3+} and Cr^{3+} luminescent ions should be excited independently to provide YAG nanothermometers with a high relative thermal sensitivity in the physiological temperature range. However, the excitation wavelength should lie in the biological transparency window, for in-depth imaging, which is not the case when using a 532 nm excitation. Marciniak *et al.* propose to use a 590-nm excitation wavelength [30], allowing both the excitation of Cr^{3+} in the $^4A_2$ band and the excitation of Nd^{3+} in the $^2G_{7/2}$ level and coming closer to the biological window. To shift the excitation to an even higher wavelength, the $^4I_{9/2} \rightarrow {}^4F_{9/2}$ transition of

Nd^{3+}, centered around 680 nm, should be targeted. However, at 680 nm, the absorption coefficient of Cr^{3+}-doped YAG matrix is weak [41]. Thus, a more appropriate host matrix should be selected, such as $Y_3Al_2Ga_3O_{12}$ [48] or $Gd_3Sc_2Al_3O_{12}$ [49], allowing both the excitation of Cr^{3+} and Nd^{3+} simultaneously under the 680-nm excitation.

5. Conclusion

Temperature-dependent luminescence properties of Nd^{3+},Cr^{3+}-codoped YAG nanocrystals have been studied under two excitation mechanisms: one consisting in exciting Cr^{3+} ions, which further transfer their excitation to Nd^{3+} ions, and the other which allows the direct and independent excitation of both Nd^{3+} and Cr^{3+} ions. In the first case, the thermal sensing depends on the temperature-dependence of phonon-assisted energy transfer, whereas, in the second case, it depends on the difference of thermal behaviors of two types of doping ions (one transition metal ion and one lanthanide ion) in the considered temperature range. In the case of these YAG nanocrystals, the latter process leads to the highest relative thermal sensitivity (S_r = 2.5 %.K^{-1}) in the physiological temperature range, under a 532 nm excitation. However, thermal sensing based on phonon-assisted energy transfer could turn out to be highly efficient in some host matrices [50], especially when working with smaller nanocrystals where phonons from surface groups can play a fundamental role in the energy transfers.

Acknowledgments

G.D. acknowledges French National Research Agency for funding (project NanophosforLED, ANR-17-CE09-0035-01).

[1] L. Aigouy, G. Tessier, M. Mortier, B. Charlot, Scanning thermal imaging of microelectronic circuits with a fluorescent nanoprobe. *App. Phys. Letters* (2005) **87**, 184105. DOI: 10.1063/1.2123384

[2] P. Low, B. Kim, N. Takama, C. Bergaud, High-Spatial-Resolution Surface-Temperature Mapping Using Fluorescent Thermometry. *Small* (2008) **4**, 908–914. DOI:10.1002/smll.200700581

[3] F. Vetrone, R. Naccache, A. Zamarron, A. Juarranz de la Fuente, F. Sanz-Rodrıguez, L.Martinez Maestro, E. Martın Rodriguez, D. Jaque, J.Garcıa Sole, J.A. Capobianco, Temperature Sensing Using Fluorescent Nanothermometers. *ACS Nano*, (2010) **4(6)** 3254–3258. DOI: 10.1021/nn100244a

[4] K. M McCabe, M. Hernandez, Molecular Thermometry. *Pediatric Research volume* (2010) **67** 469–475

[5] S. Freddi, L. Sironi, R. D'Antuono, D. Morone, A. Donà, E. Cabrini, L. D'Alfonso, M. Collini, P. Pallavicini, G. Baldi, D. Maggioni, G. Chirico, A Molecular Thermometer for Nanoparticles for Optical Hyperthermia. *NanoLett.* (2013) **13** 2004−2010. DOI: 10.1021/nl400129v

[6] S. Uchiyama, C. Gota, T. Tsuji, N. Inada, Intracellular temperature measurements with fluorescent polymeric thermometers. *Chem. Comm.* (2017) **53** 10976-10992. DOI: 10.1039/C7CC06203F

[7] D. Macherel, F. Haraux, H. Guillou, O. Bourgeois, The conundrum of hot mitochondria. *BBA - Bioenergetics* (2021) **1862**, 148348. DOI: 10.1016/j.bbabio.2020.148348

[8] C.D.S. Brites, P.P. Lima, N.J.O. Silva, A. Millán, V.S. Amaral, F. Palacio, L.D. Carlos, Thermometry at the nanoscale. *Nanoscale* (2012) **4** 4799–4829. DOI: 10.1039/c2nr30663h

[9] C.D.S. Brites, S. Balabhadra, L.D. Carlos. Lanthanide-Based Thermometers: At the Cutting-Edge of Luminescence Thermometry. *Adv. Optical Mater.* (2018) 1801239. DOI : 10.1002/adom.201801239

[10] K. Iwai, Y. Matsumura, S.Uchiyama, A. P. de Silva. Development of fluorescent microgel thermometers based on thermo-responsive polymers and their modulation of sensitivity range. *Mater. Chem.,* (2005) **15** 2796–2800. DOI: 10.1039/B502277K

[11] S. Uchiyama, A.P. de Silva, K. Iwai, Luminescent molecular thermometers. *J. Chem. Educ.* (2006) **83** 720–727. DOI: 10.1021/ed083p720

[12] Z.Gan, X. Wu, J. Zhang, X. Zhu, P.K. Chu. In Situ Thermal Imaging and Absolute Temperature Monitoring by Luminescent Diphenylalanine Nanotubes, *Biomacromolecules* (2013) **14** 2112−2116 - 10.1021/bm400562c

[13] J.S. Donner, S.A. Thompson, M.P. Kreuzer, G. Baffou, R. Quidant, Mapping Intracellular Temperature Using Green Fluorescent Protein. *Nano Lett.* (2012) **12** 2107-2111. DOI: 10.1021/nl300389y

[14] A.M. Kaczmarek, J. Liu, B. Laforce, L. Vincze, K. Van Hecke, R. Van Deun, Cryogenic luminescent thermometers based on multinuclear Eu3+/Tb3+ mixed lanthanide polyoxometalates. *Dalton* (2017) **46** 5781-5785

[15] V. Trannoy, A.N. Carneiro Neto, C.D.S. Brites, L.D. Carlos, H. Serier-Brault, Engineering of Mixed Eu3+/Tb3+ Metal-Organic Frameworks Luminescent Thermometers with Tunable Sensitivity. *Adv. Optical Mater.* (2021) **9** 2001938. DOI: 10.1002/adom.202001938

[16] S. Sekiyama, M. Umezawa, S. Kuraoka, T. Ube, M. Kamimura, K.Soga, Temperature Sensing of Deep Abdominal Region in Mice by Using Over-1000 nm Near-Infrared Luminescence of Rare-Earth-Doped NaYF Nanothermometer. *Sc. Reports* (2018) **8** 16979. DOI: 10.1038/s41598-018-35354-y.

[17] D.T. Klier, M.U. Kumke, Upconversion NaYF4:Yb:Er nanoparticles co-doped with Gd^{3+} and Nd^{3+} for thermometry on the nanoscale. *RSC Adv.* (2015) **5** 67149. DOI: 10.1039/C5RA11502G

[18] R. Liang, R. Tian, W. Shi, Z. Liu, D. Yan, M. Wei, D.G. Evans, X. Duan, A temperature sensor based on CdTe quantum dots–layered double hydroxide ultrathin films via layer-by-layer assembly. *Chem. Commun.* (2013) **49** 969-971. DOI: 10.1039/C2CC37553B

[19] E. Glais, A. Maitre, B. Viana, C. Chaneac, Experimental measurement of local high temperature at the surface of gold nanorods using doped ZnGa2O4 as a nanothermometer. *Nanoscale Adv.* (2021) **3** 2862. DOI: 10.1039/D1NA00010A

[20] P. Cortelletti, C. Facciotti, I.X. Cantarelli, P. Canton, M. Quintanilla, F. Vetrone, A. Speghini, M. Pedroni, Nd3+ activated CaF2 NPs as colloidal nanothermometers in the biological window. *Optical Materials* (2017) **68** 29-34. DOI: 10.1016/j.optmat.2016.11.019

[21] B. del Rosal, U. Rocha, E.C. Ximendes, E. Martín Rodríguez, D. Jaque, J. García Sole, Nd3+ ions in nanomedicine: Perspectives and applications. *Optical Materials* (2017) **63** 185-196. DOI: 10.1016/j.optmat.2016.06.004

[22] Antonio Benayas, Blanca del Rosal, Alberto Pérez-Delgado, Karla Santacruz-Gómez, Daniel Jaque, Gustavo Alonso Hirata, and Fiorenzo Vetrone, Nd:YAG Near-Infrared Luminescent Nanothermometers. *Adv. Optical Mater.* (2015) **3** 687–694. DOI: 10.1002/adom.201400484

[23] G. Dantelle, M. Matulionyte, D. Testemale, A. Cantarano, A. Ibanez, F. Vetrone, Nd3+ doped Gd3Sc2Al3O12 nanoparticles: towards efficient nanoprobes for temperature sensing, *Phys. Chem. Chem. Phys.* (2019) **21** 11132-11141. DOI: 10.1039/c9cp01808e

[24] M. Suta, Ž. Antic, V. Đorđevic, S. Kuzman, M.D. Dramicanin, A. Meijerink, Making Nd^{3+} a Sensitive Luminescent Thermometer for Physiological Temperatures—An Account of Pitfalls in Boltzmann Thermometry, *Nanomaterials* (2020) **10** 543. DOI:10.3390/nano10030543

[25] A. Skripka, A. Morinvil, M. Matulionyte, T. Cheng, F. Vetrone, Advancing neodymium single-band nanothermometry. *Nanoscale* (2019) **11** 11322. DOI: 10.1039/C9NR02801C

[26] B. del Rosal, E. Ximendes, U. Rocha, D. Jaque, In Vivo Luminescence Nanothermometry: from Materials to Applications. *Adv. Optical Mater.* (2016) **5** 1600508. DOI: 10.1002/adom.201600508

[27] Ł. Marciniak, A. Bednarkiewicz, M. Stefanski, R. Tomala, D. Hreniak and W. Strek, Near infrared absorbing near infrared emitting highly-sensitive luminescent nanothermometer based on Nd^{3+} to Yb^{3+} energy transfer. *Phys. Chem. Chem. Phys.* (2015) **17** 24315. DOI: 10.1039/C5CP03861H

[28] A.F. Silva, F. Elan, E.L. Falcao-Filho, L.J.Q. Maia, C.B. de Araujo, Thermal sensitivity of frequency upconversion in $Al_4B_2O_9$:Yb^{3+}/Nd^{3+} nanoparticles. *J. Mater. Chem. C* (2017) **5** 1240. DOI: 10.1039/C6TC04630D

[29] A. Skripka, A. Benayas, R. Marin, P. Canton, E. Hemmer and F. Vetrone, Double rare-earth nanothermometer in aqueous media: opening the third optical transparency window to temperature sensing. *Nanoscale* (2017) **9** 3079. DOI: 10.1039/C6NR08472A

[30] L. Marciniak, A. Bednarkiewicz, D. Kowalska, W. Strek, A new generation of highly sensitive luminescent thermometers operating in the optical window of biological tissues. *J. Mater. Chem. C* (2016) **4** 5559-5563. DOI: 10.1039/C6TC01484D

[31] K. Elzbieciak, L. Marciniak, The Impact of Cr^{3+} Doping on Temperature Sensitivity Modulation in Cr^{3+} Doped and Cr^{3+}, Nd^{3+} Co-doped $Y_3Al_5O_{12}$, $Y_3Al_2Ga_3O_{12}$, and $Y_3Ga_5O_{12}$ Nanothermometers. *Frontiers in Chemistry* (2018) **6** 424. DOI: 10.3389/fchem.2018.00424

[32] K. Kniec, M. Tikhomirov, B. Pozniak, K. Ledwa, L. Marciniak, $LiAl_5O_8$:Fe^{3+} and $LiAl_5O_8$:Fe^{3+}, Nd^{3+} as a New Luminescent Nanothermometer Operating in 1st Biological Optical Window. *Nanomaterials* (2020) **10** 189. DOI:10.3390/nano10020189

[33] J. Drabik, B. Cichy, L. Marciniak, New Type of Nanocrystalline Luminescent Thermometers Based on Ti3+/Ti4+ and Ti4+/Ln3+ (Ln3+ = Nd3+, Eu3+, Dy3+) Luminescence Intensity Ratio. *J. Phys. Chem. C* (2018) **122** 14928−14936. DOI: 10.1021/acs.jpcc.8b02328

[34] K. Trejgisa, M.D. Dramićaninb, L. Marciniak. Highly sensitive multiparametric luminescent thermometer for biologically-relevant temperatures based on Mn4+, Ln3+ co-doped SrTiO3 nanocrystals. *Journal of Alloys and Compounds* (2021) **875** 159973. DOI: 10.1016/j.jallcom.2021.159973

[35] K. Elzbieciak-Piecka, C. Matuszewskaand L. Marciniak, Step by step designing of sensitive luminescent nanothermometers based on Cr3+,Nd3+co-dopedLa3-xLuxAl5-yGayO12nanocrystals. *New J. Chem.* (2019) **43** 12614-12622. DOI: 10.1039/C9NJ03167G

[36] L. Marciniak, A. Bednarkiewicz, J. Drabik, K. Trejgis, W. Strek, Optimization of highly sensitive YAG:Cr^{3+},Nd^{3+} nanocrystals based luminescent thermometer operating in optical window of biological tissues. *Phys. Chem. Chem. Phys.* (2017) **19** 7343-7351. DOI: 10.1039/C6CP07213E

[37] L. Marciniak, A. Bednarkiewicz, W. Strek. The impact of nanocrystals size on luminescent properties and thermometry capabilities of Cr, Nd doped nanophosphors. *Sensors and Actuators B* (2017) **238** 381–386. DOI: 10.1016/j.snb.2016.07.080

[38] G. Dantelle, D. Testemale, E. Homeyer, A. Cantarano, S. Kodjikian, C. Dujardin, J.L. Hazemann, A. Ibanez. A new solvothermal method for the synthesis of size-controlled YAG:Ce single-nanocrystals. *RSC Advances* (2018) **8** 26857-26870. DOI: 10.1039/c8ra05914d

[39] D. Hreniak, W. Strek, P. Głuchowski, R. Fedyk, W. Łojkowski, The Concentration Dependence of Luminescence of Nd:$Y_3Al_5O_{12}$ Nanoceramics. *J Alloy Compd* (2008) **451** 549-552. DOI: 10.1016/j.jallcom.2007.04.137

[40] D. Testemale, R. Argoud, O. Geaymond, J.L. Hazemann, High pressure/high temperature cell for x-ray absorption and scattering techniques. *Review of Scientific Instruments* (2005) **76** 043905.

[41] P. Guchowski, R. Pazik, D. Hreniak, W. Strek, Luminescence properties of Cr^{3+}:Y3Al5O12 nanocrystals. *J. Lumin.* (2009) **129** 548–553. DOI: 10.1016/j.jlumin.2008.12.012

[42] E. Hemmer, A. Benayas, F. Legare and F. Vetrone, Exploiting the Biological Windows: Current Perspectives on Fluorescent Bioprobes Emitting above 1000 nm. *Nanoscale Horiz.,* (2016) **1** 168–184. DOI:10.1039/C5NH00073D

[43] G. Blasse, B.C. Grabmaier, B.C, Luminescent Materials, Springer-Verlag, Berlin (1994)

[44] H. Zhang, D. Sun, J. Luo, Z. Fang, X. Zhao, C. Quan, L. Hu, M. Cheng, Qi. Zhang, S. Yin, Influence of Cr^{3+} doping on the spectroscopies and laser performance of Cr,Nd:YAG crystal operated at 1.06 μm. *Optical Engineering* (2019) **58(2)** 027116 DOI:10.1117/1.OE.58.2.027116

[45] P. Pichon, A. Barbet, D. Blengino, P. Legavre, T. Gallinelli, F. Druon, J.-P. Blanchot, F. Balembois, S. Forget, S. Chénais, P. Georges, High-radiance light sources with LED-pumped luminescent concentrators applied to pump Nd:YAG passively Q-switched laser. *Optics and Laser Technology* (2017) **96** 7–12

[46] Y. Honda, S. Motokoshi, T. Jitsuno, N. Miyanaga, K. Fujioka, M. Nakatsuka, M. Yoshida. Temperature dependence of optical properties in Nd/Cr:YAG materials. *Journal of Luminescence* (2014) 148, 342–346. DOI: 10.1016/j.optmat.2019.02.032

[47] Y. Honda, S. Motokoshi, T. Jitsuno, K. Fujioka, M. Nakatsuka, M. Yoshida, T. Yamada, J. Kawanaka, N. Miyanaga. Temperature-dependent fluorescence decay and energy transfer in Nd/ Cr:YAG ceramics. Optical Materials (2019) 90, 215-219. DOI: 10.1016/j.optmat.2019.02.032

[48] Z. Dai, V. Boiko, M. Markowska, A. Gerus, K. Grzeszkiewicz, J. Holsa, M.L. Saladino, D. Hreniak, Optical studies of Y3(Al,Ga)5O12:Ce3+,Cr3+,Nd3+ nano-phosphors obtained by the Pechini method. Journal of Rare Earths, (2019) 37 1132-1136. DOI: 10.1016/j.jre.2019.04.006

[49] L.S. Sumida, M.S. Mangir, D.A. Rockwell, M. D. Shinn, Laser-related properties of chromium-and neodymium-doped gadolinium scandium aluminum garnet (Cr:Nd:GSAG). *J. Opt. Soc. America B* (1994) **11** 2066-2078 DOI:10.1364/JOSAB.11.002066

[50] W. Ye, Y. Wang, C. Zhao, Z. Wen, Z. Cao, Z. Cao, X. Shen, Y. Li, X. Yuan, C. Wang, C. Ma, Y. Cao, Optical temperature sensing based on phonon-assisted population of Dy3+sensitized by Gd3+in Gd2Ge2O7 nanophosphors. *J. Lum.* (2020) **227** 117567. DOI: 10.1016/j.jlumin.2020.117567